LASER INTERFEROMETER GRAVITATIONAL WAVE OBSERVATORY

LIGO Laboratory / LIGO Scientific Collaboration

LIGO-T060083-01-D *ADVANCED LIGO* 06/01/07

Auxiliary Optics Support System Conceptual Design Document, Vol. 1 Thermal Compensation System

Michael Smith, Phil Willems

Distribution of this document:
LIGO Scientific Collaboration

This is an internal working note
of the LIGO Project.

California Institute of Technology
LIGO Project – MS 18-34
1200 E. California Blvd.
Pasadena, CA 91125
Phone (626) 395-2129
Fax (626) 304-9834
E-mail: info@ligo.caltech.edu

Massachusetts Institute of Technology
LIGO Project – NW17-161
175 Albany St
Cambridge, MA 02139
Phone (617) 253-4824
Fax (617) 253-7014
E-mail: info@ligo.mit.edu

LIGO Hanford Observatory
P.O. Box 1970
Mail Stop S9-02
Richland, WA 99352
Phone 509-372-8106
Fax 509-372-8137

LIGO Livingston Observatory
P.O. Box 940
Livingston, LA 70754
Phone 225-686-3100
Fax 225-686-7189

http://www.ligo.caltech.edu/

Table of Contents

Table of Figures

1 Version History for this Document

Sep. 20, 2006- -00 Initial release.

June 1, 2007- -01 Rewrite, with revised TCS strategy, no ring heaters on the CP, revised CP dimensions, and downselect of Hartmann sensors.

2 Past Experience with Thermal Compensation

Thermal compensation has been an essential part of LIGO operation since 2004. At that time, it was recognized that the 'point design' approach to core optics polishing, in which the optics are polished in such a way as to thermally distort into the optimal radius of curvature at the interferometer's operating power level, was not adequate for interferometer commissioning and operation. So, a CO_2 laser projector was designed and installed, first on the H1 interferometer (the most overheated), and subsequently on L1 and H2. This CO_2 laser projector was retrofitted into the interferometers to shine through ZnSe viewports installed on the beam tube and illuminate the HR faces of the ITMs. A schematic of the initial LIGO CO_2 laser projector can be found in the report on the initial LIGO TCS experience[1].

The installation of TCS gave enormous flexibility to the operation of the interferometers. They could be run below full operating power, yet with the optics centrally heated to deform them into ideal alignment. Interferometers that overheated (such as H1, before its lossy optics were replaced and cleaned) could have compensating annular heat provided to the same end. And, it was found that the unwanted AS_I signal could be substantially reduced by appropriate differential heating between the two arms.

As useful as TCS has been, its implementation is far from ideal. Because the heating is applied to the HR faces of the ITMs, noise in the TCS lasers can sometimes be seen in the interferometer signal through coupling to thermorefractive and thermelastic response of the ITM surfaces. Also, the amount of heat power available from the TCS tables is less than has been required at times. Lastly, the absence of any useful sensor to analyze the thermally distorted phase profiles of the optics has made the design of the appropriate heating pattern a matter of guesswork. Even to determine which optic was overheating in the seriously overheated H1 took months of effort.

The design of the initial LIGO TCS was loosely based upon the research done by Ryan Lawrence for his Ph.D. research at MIT, in which he analyzed the various problems thermal aberration could produce in GW interferometers and demonstrated two alternative yet complementary compensators: shielded ring heaters and scanned CO_2 laser projectors. The retrofit of ring heater into initial LIGO was deemed too invasive, and the scanned CO_2 laser projector as he designed it would have injected too much noise into the interferometer. Also, his scanned CO_2 laser projector relied on an optic phase profile measurement to close a feedback loop.

Thermal compensation will be an even more essential part of Advanced LIGO, due to the much greater circulating laser power it will use. This document outlines a strategy for successfully implementing TCS in Advanced LIGO in such a way as to satisfy the performance requirements detailed in the TCS Design Requirements Document.

[1] "Thermal Compensation Design Description," Stefan Ballmer *et al.*, LIGO-T050064-00-R.

3 Overall Design

3.1 Design Philosophy

The Thermal Compensation System (TCS) will correct for a wide range of thermal effects in the interferometer, arising in several optics. While significant effort into reducing the coating and substrate absorptions is underway, TCS provides the most flexibility for corrections should some optic not meet specifications. In addition, TCS provides an online tool for correcting mirror radius errors, and can be used to suppress acoustic parametric instabilities by controlling the transverse mode spectrum of the arm cavities. Finally, while TCS has the capability to correct for inhomogeneities in optical absorption, it is not possible to specify their size or distribution in advance.

For these reasons, TCS will be designed with as much flexibility as possible. In addition, the value of being able to easily measure the thermal aberrations for individual optics was demonstrated by its lack in initial LIGO, so TCS will implement sensors, both on individual core optics, and on the main interferometer beam.

The design philosophy for TCS reflects the choice of fused silica for the test mass substrates in Advanced LIGO. It assumes further that the mirror radii of curvature are optimized for cold operation.

3.2 Overall Layout of TCS

[Includes revisions to the conceptual design developed since the CDR, noted in boldface.]

The positions of the thermal compensators and optical sensors are indicated schematically in Figure 1. The phase cameras monitoring pickoff ports of the main interferometer beam are not shown.

The main thermal compensation of homogeneous absorption in the optics will use carbon dioxide laser projectors (**revised from shielded ring heaters in version 00**), acting upon compensation plates suspended from the reaction chains of the ITM quadruple suspensions.[2] Calculations have shown that the noise injected by, and power required from, a CO_2 laser projector are obtainable using available technology.[3] Compensation and control of the TM HR surfaces will be done by shielded ring heaters mounted within the quad SUS structure. For each interferometer, there are four of these: one around each test mass, toward the AR face (**reduced from six in version 00**). The test mass ring heaters will control the arm cavity mode shape. The ITM ring heaters will also provide limited compensation of thermorefractive aberration in the recycling cavities. The test mass ring heaters might also be used to temperature-tune away radiation-pressure parametric instabilities.

In his thesis, Ryan Lawrence showed two advantages to applying the thermal compensation to a compensation plate, rather than to the input test mass directly. First, optimum compensation

[2] RODA : CP to be the Ultimate Mass in the ITM Reaction Chain, LIGO document LIGO-M040005-01-Y.

[3] TCS Actuator Noise Coupling, LIGO document LIGO-T060224-00-D.

requires a zero net heat flow on the barrel of the compensated optic[4]. This is much more conveniently done to a compensation plate than a test mass, although the thermal interaction between the ITM and CP will likely require some form of insulation of the test mass barrel, using a low-emissivity coating or shield.[5] Second, since the compensation plate lives entirely within the recycling cavity and has no HR surfaces, the effect of compensator noise is much less important on a compensation plate than on a test mass. The disadvantage to the compensation plate is that it cannot compensate errors within the arm cavities.

Carbon dioxide laser projectors can provide compensation of non-axisymmetric thermal lensing. These projectors will be located outside the vacuum envelope for easy modification of the projected thermal profile.

Each optic with a significant thermal load will be independently monitored. The HR face of each test mass will be monitored in reflection for deformation. The input test mass/compensation plate phase profile will be monitored on reflection on-axis from the recycling cavity side. On-axis sensing requires that the probe beam enter the recycling cavity through a pickoff port, such as the wedged AR face of the beamsplitter. Lastly, while no compensation on or near the beamsplitter is proposed, it does contribute about 10% of the thermal aberration in the interferometer, and so is monitored in transmission. The beamsplitter monitor could be made unnecessary if special low-absorption glass is used for the beamsplitter, making its thermal lens negligible.

Knowledge of the phase profile of each optic is valuable, but the most important quantity is the mode profile of the interferometer beam. This will be monitored, using phase cameras, at pickoff ports of the interferometer.

[4] Heat flow out the barrel implies a radial thermal gradient there, which in turn would cause a thermorefractive optical phase gradient.

[5] Heating of the ITM by the Compensation Plate in Advanced LIGO, LIGO document LIGO-T070123-00-D.

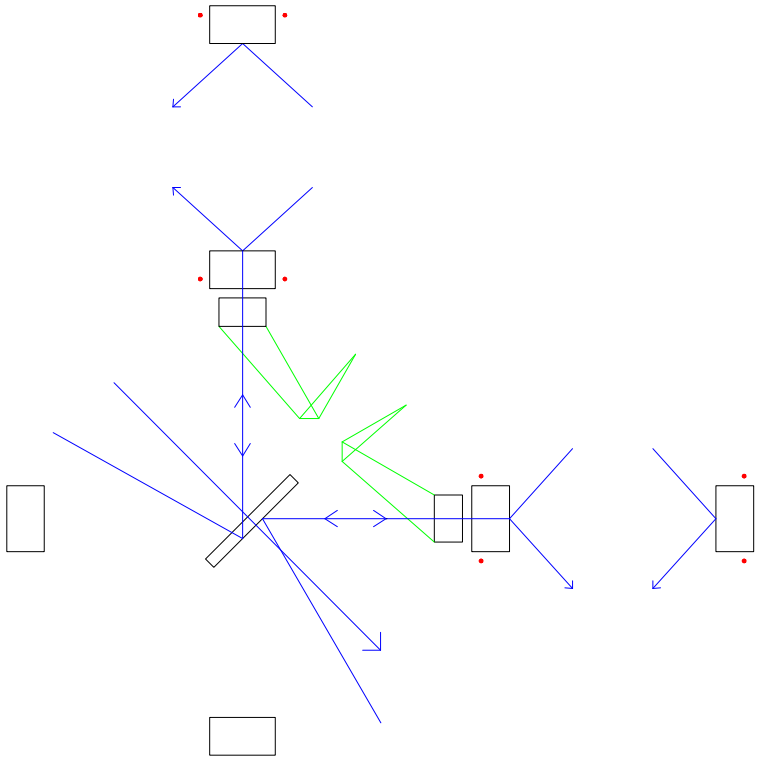

Figure 1: layout of thermal compensators and thermal compensation sensors. Red dots: shielded ring heaters. Blue arrows: optical path sensors (Hartmann sensors). Green projections: carbon dioxide laser heaters.

The thermal aberrations will be sensed by several complementary techniques. To lowest order, the degree of aberration will be manifest in IFO channels such as SPOB and AS_I, as it is in initial LIGO. These are scalar quantities that reflect only the overall conversion of light from the fundamental cavity mode. To sense the spatial structure of the cavity mode, phase cameras and Spiricons will sample the interferometer beam at several ports. However, the use of spatial sensors to actively control thermal aberrations has not yet been demonstrated, and the coupled cavity nature of the IFO will make extracting the aberrations of individual mirrors very problematic. Therefore, wavefront sensors will probe the input test masses and beamsplitter individually. The final TCS control will likely adopt a blend of these sensors as inputs.

Figure 2 shows this control scheme for the TCS system in a block diagram.

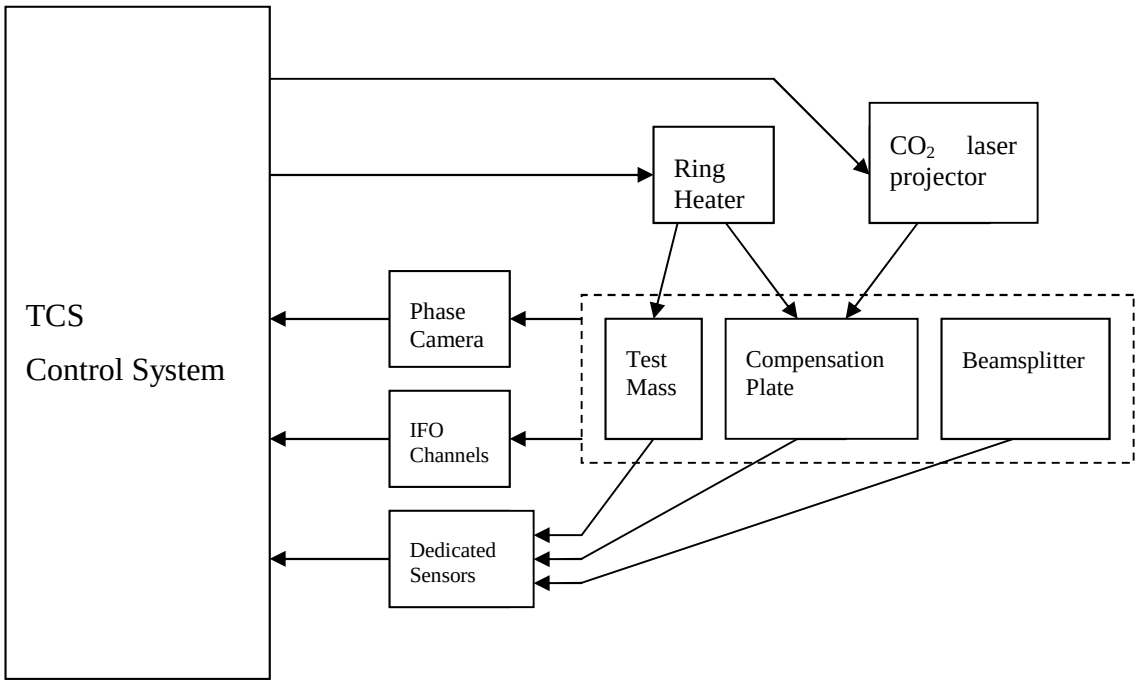

Figure 2: Block diagram of the TCS system.

4 TCS Elements

4.1 Actuators

4.1.1 Test Mass Ring Heater

The self-heating of the test masses will be predominantly through absorption in the HR coatings. This will raise a bump in the center of the test mass faces, making their surface profile non-spherical. The cavity becomes less concentric, and the spot sizes at the mirrors will shrink. However, given uniform absorption at the .5 ppm level expected in Advanced LIGO, this departure from sphericity will not make the arm cavity resonant modes significantly non-Gaussian. Figure 3 shows the surface deformation caused by .5 ppm absorption, and Figure 4 the resulting arm cavity mode, along with the best-fit Gaussian of 5.4 cm spot size.

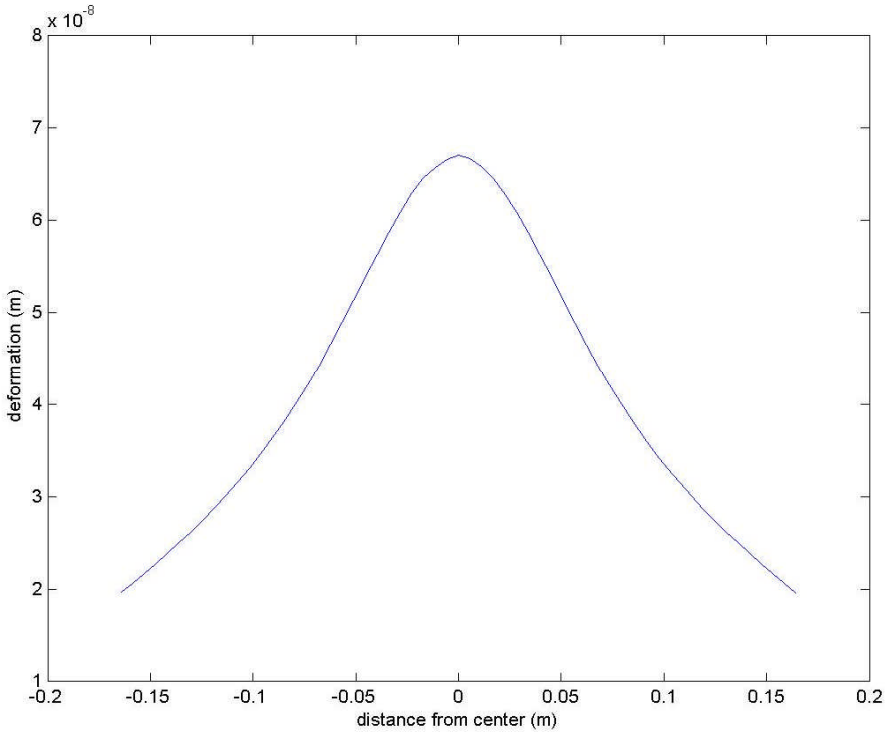

Figure 3: TM surface deformation due to interferometer self-heating, and resultant arm cavity mode intensity profile. In the arm cavity mode plot, the simulation is in green, and the best fit gaussian in red.

Assuming .5 ppm absorption per coating on each test mass, the ITM spot size will vary from 6 cm at low power to 5.4 cm at full power. We may decide to live with this variation, although the increase in thermal noise level involved is of order 15%. However, should we choose to maintain the arm cavity mode structure, we must control the radii of curvature of all test masses.

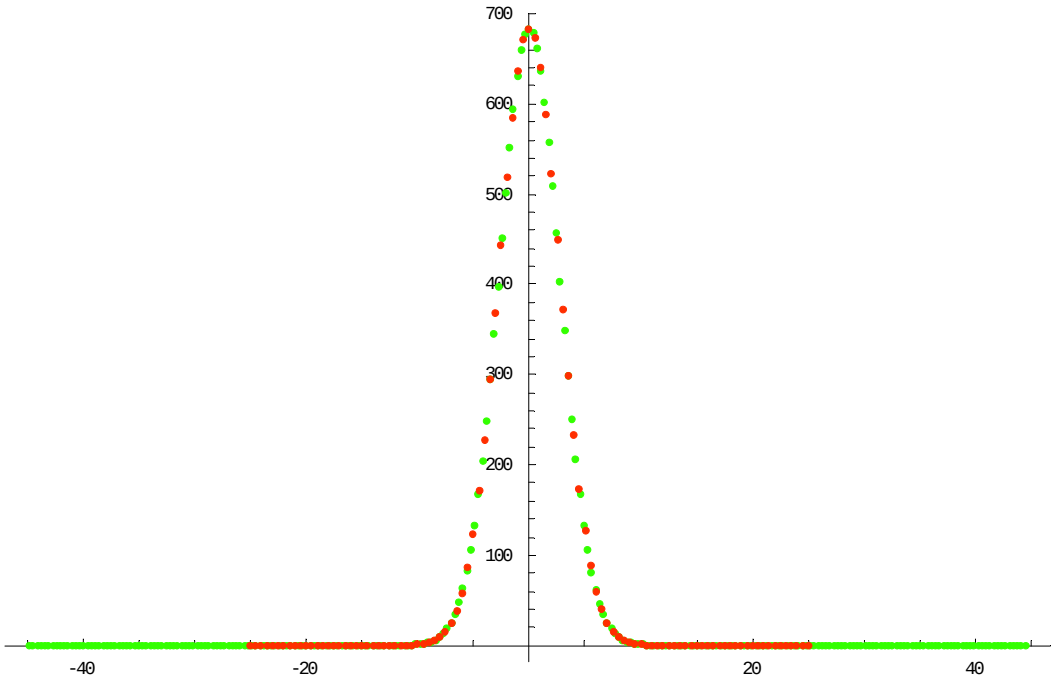

Figure 4: Arm cavity mode intensity profile resulting from the deformation in Figure 3. The simulation is in green, and the best fit gaussian in red.

A conceptual design of the test mass ring heater is shown in Figure 5.

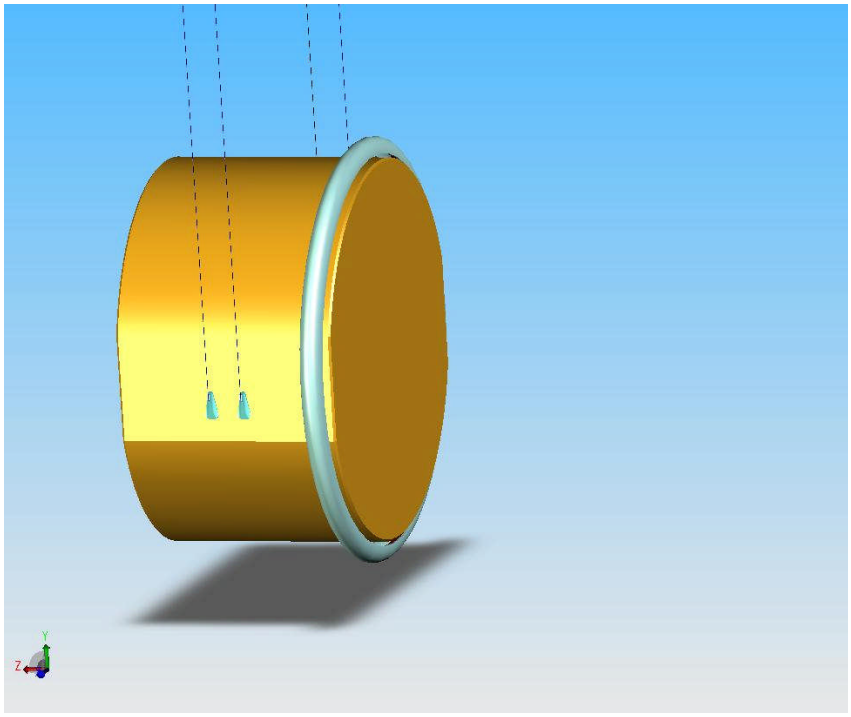

Figure 5: suspended test mass with shielded ring heater in position. The ring heater is inside the parabolic shield and not visible- neither is the mount holding the ring and shield to the suspension cage.

This ring heater has dimensions 360 mm diameter, 5 mm thickness. The shield around the ring heater is a revolved parabola with the ring at the focus, 20 mm wide, extending to within 4 mm of the test mass barrel. The design is axisymmetric; whether to modify the ring or shield near the optic flats has not been considered. It will be mounted near the AR face of the optic, with precise position and means to be determined in consultation with SUS.

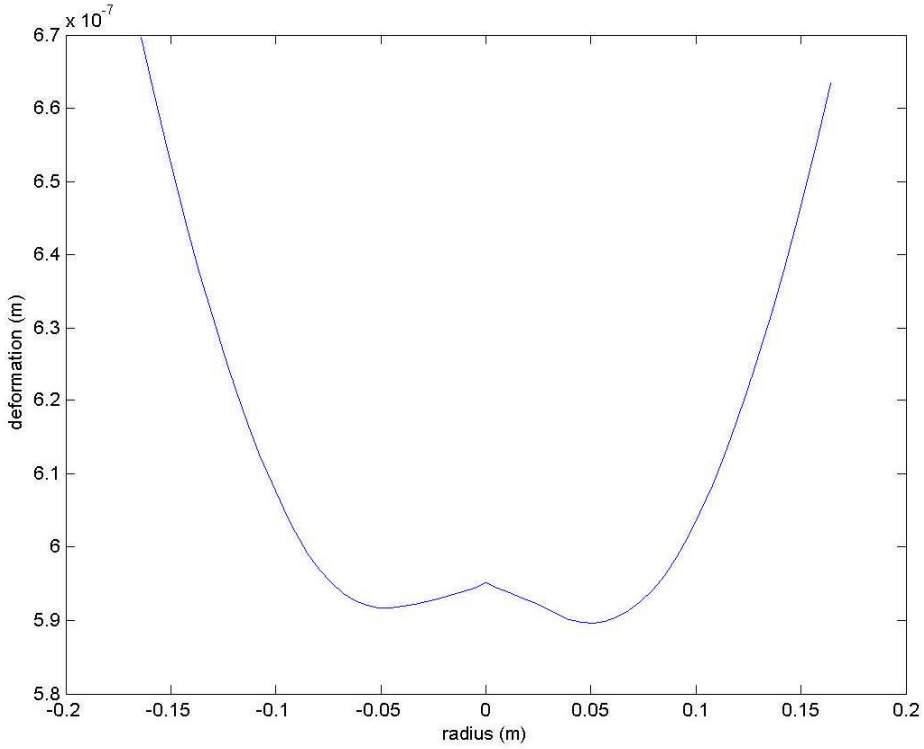

Figure 6: ring compensated test mass thermoelastic HR surface deformation.

The thermal deformation of the HR surface of the test mass due to heating near the AR face is nearly insensitive to the precise distribution of heat, being essentially a spherical concavity. The total thermoelastic deformation for optimized compensation is shown in **Error! Reference source not found.**, along with the resulting arm cavity mode structure in Figure 7. While the surface deformation has not been thoroughly corrected (that would be a flat profile), the resulting intensity pattern is very close to the fundamental Gaussian of 6 cm spot size at the ITM. Close inspection shows that the compensated mode has slightly more power at large radius than does the Gaussian- the round-trip diffraction loss for this mode is 22 ppm, as opposed to <1 ppm for the Gaussian, and the overlap with the Gaussian is 99.977%. The amount of heat required to achieve compensation was 11W incident upon the optic. Given the close proximity and good coverage of the (reflective) shield, we can assume that most of the radiated ring power will be incident on the optic. The radiated power is about .1 W/cm, much less than the 2.5 W/cm for which the blackbody spectrum

from a ring heater shifts into the transmissive band of fused silica.[6] We propose that this heater should provide up to 22W to the optic if needed. This conceptual design satisfies the requirement in Section 3.1.2.1 of the TCS DRD.

The application of heat directly to the test mass will change the thermorefractive phase profile inside the test mass, and thus the thermal aberration inside the recycling cavity. Figure 8 shows the thermal phase maps for reflection from the AR side of the ITM, with and without the thermal compensation from a test mass ring heater. This phase profile can be compensated, but only with the CO_2 laser projector, and only if the projector runs at the very best intensity stability we think might be achievable. Therefore, the preferred strategy is to maintain the 6 cm spot size at the ITM by acting solely on the ETM through its ring heater. This strategy is outlined in LIGO document T060214-01-D; the noise coupling analysis that indicates that the CO_2 laser projector intensity noise would be barely adequate is in LIGO document T060224-00-D.

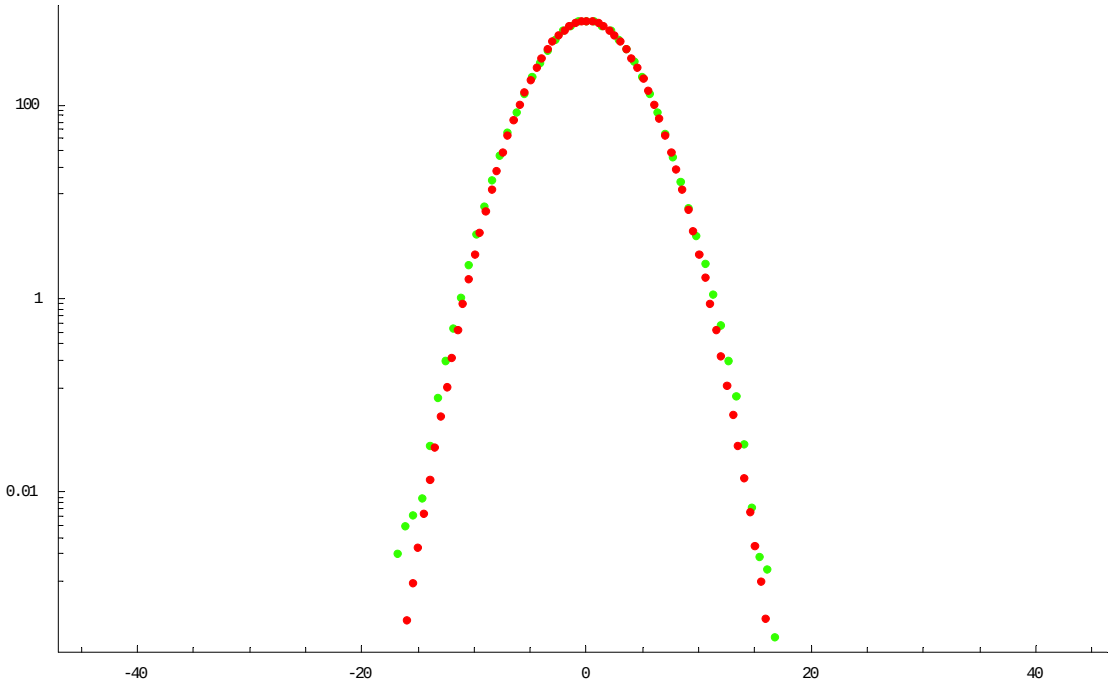

Figure 7: Arm cavity mode intensity profile resulting from surface deformation in Figure 6. As before, the FFT simulation is in green, and the best-fit Gaussian (with 6 cm spot size at ITM) in red.

This design is less sensitive to actuator noise fluctuations than designs that heat the optic's face, because the heating is entirely on the barrel far from the IFO beam, and the radiation pressure averages to zero over the mass. However, there is a slight coupling of overall power fluctuations to HR surface displacement, because power fluctuations create fluctuations in the flexure of the mirror, which cause fluctuations in the position of the HR surface relative to the mirror's center of mass. This noise coupling is discussed in Section 8.1.

[6] Lawrence's thesis, p. 215.

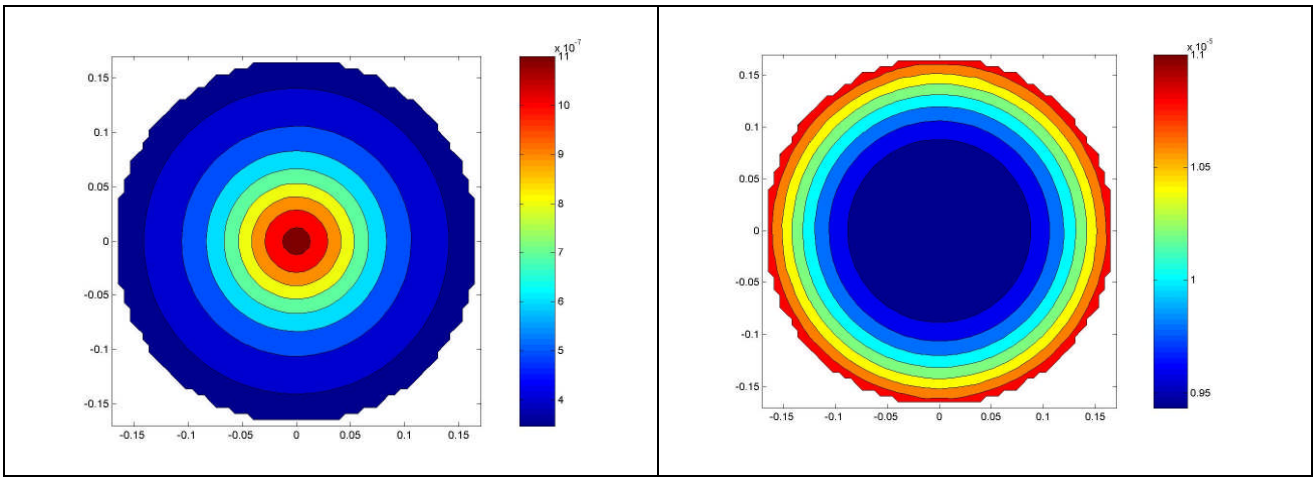

Figure 8: Phase profiles through directly heated ITM, without (left) and with (right) test mass ring heater compensation.

4.1.2 Compensation Plate

The compensation plate will receive thermal actuation to compensate thermal aberration effects in the recycling cavities. This actuation will come from the CO_2 laser projector outside the vacuum. The CO_2 laser projector heating pattern is easily reconfigurable and should allow for fairly rapid characterization and improvement. From Lawrence's thesis until recently, it had been expected to use shielded ring heaters on the compensation plate as well. The shielded ring heater could provide quiet power compared to the CO_2 laser projector, due to the ring's inherent thermal averaging of input power fluctuations. However, the noise couplings on the compensation plate admit use of a reasonably stabilized CO_2 laser, and the difficulties of accommodating the ring heater near the suspension structure (mechanical and optical interference, structure heating) made good shielded ring heater design speculative.

Use of a compensation plate for correction of thermal aberrations has been demonstrated at the High Power Test Facility at Gingin. At present there is not a detailed analysis of the quality of compensation achieved. However, Ryan Lawrence has modeled in detail the degree of compensation achievable using a ring heater on a compensation plate, and has shown in the case of purely homogeneous absorption that thermal aberration can be reduced to $10^{-4.1}$ of its uncorrected value, as measured by the scatter of power from the TEM00 mode. Estimates of the requirements for Advanced LIGO indicate that correction of the order of 10^{-3} will be required at the highest power, so compensation on a plate appears practical.

The compensation plate interacts directly with the IFO beam. As such, it must satisfy requirements like those of a core optic with respect to displacement noise, absorption and scatter, index homogeneity, antireflection coatings, and the like. In addition, the CP may provide pickoff beams for IFO sensing and control. There appears to be no difficulty in applying antireflection coatings, wedges, or compensating polishes to CPs. The CP isolation requirements are far less than those for the ITMs, so suspension from the ITM reaction chain should provide more than sufficient isolation. The CP will be suspended from two wire loops and will not have flats polished on its sides. Its

dimensions are 170 mm radius, 130 mm thick (**increased from 65 mm**)[7], and it will be made from low-absorbing Suprasil 311.

The power absorbed in the CP for 2 ppm/cm will be 36 mW, far less than the .5 W of power absorbed by the ITM, so the additional aberration it contributes will be very modest, and can be corrected along with that of the ITM.

Some improvement in the compensation could be realized at the edges by insulating the barrel of the optic (e.g. with a reflective shield or a low emissivity coating). This has not been considered in the design shown here but remains an option.

Estimates of the effect of thermal lensing on the RF sideband efficiency, arm cavity power gain, and GW sideband extraction efficiency show that it is the GW sideband extraction efficiency that sets the most stringent requirements on the quality of thermal compensation. The TEM00 mode must overlap with itself to better than about 99.9% to maintain the GW sideband output amplitude to within 5% of its nominal value.

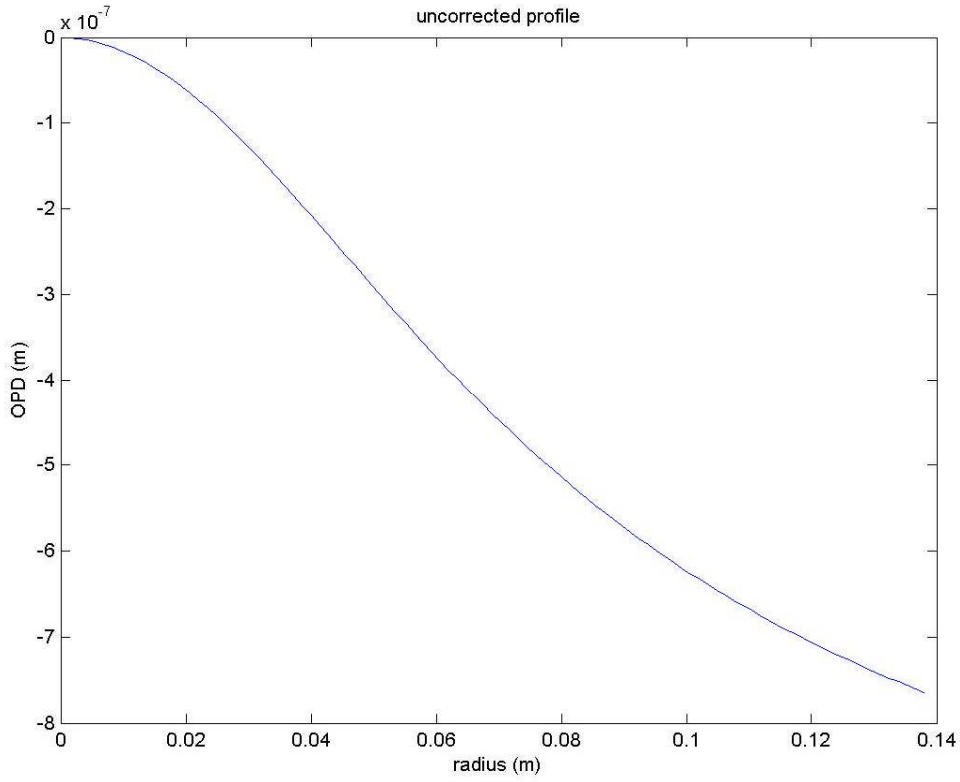

Figure 9: Radial phase profile of an uncompensated ITM at full IFO power.

[7] See RODA: Compensation Plate dimensions, LIGO document LIGO-M060305-01-Y.

The phase profile of the ITM in the recycling cavity is shown in Figure 9; along with the optimized profile from a ring heater (Figure 10) and compensated phase profile (Figure 11). This assumes the baseline ITM absorption[8], and the total TCS power incident upon the CP is 6 W. The mode overlap calculated for the TEM00 mode through the compensated optical phase profile is 99.99%, which meets the requirements in Sections 3.1.2.2, 3.1.2.3, and 3.1.2.5 of the Advanced LIGO TCS Design Requirements Document. It should be noted that the uncompensated mode overlap is only 49%. We expect a CO_2 laser projector to be easily able to generate this heating profile.

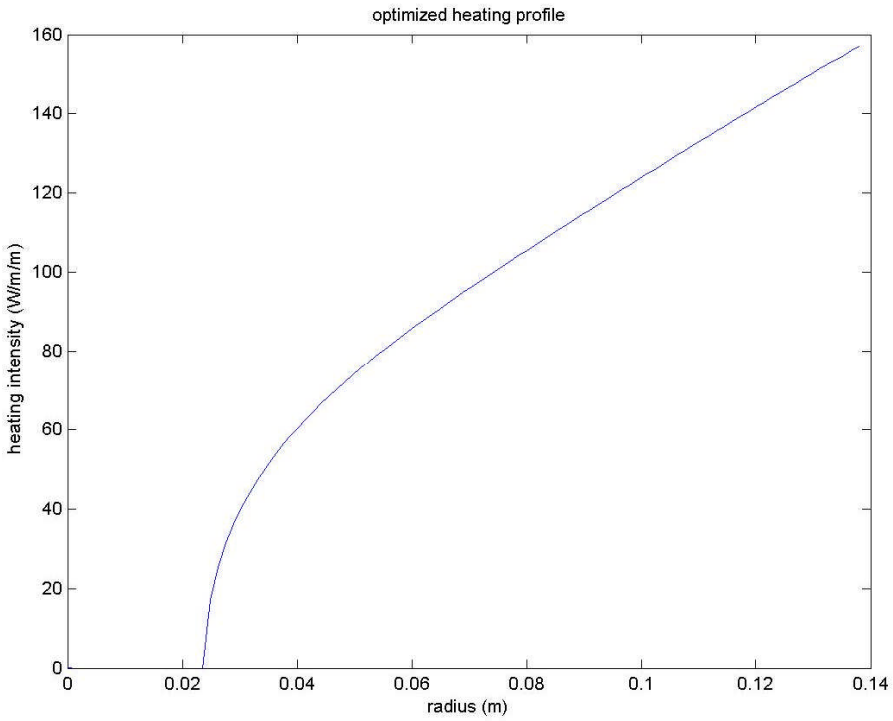

Figure 10: Compensation heating profile from optimized shielded ring heater.TCS must also minimize the stray light at the dark port, in concert with the output mode cleaner.

This is discussed in more detail in Section 7.2.

[8] 850 kW arm power and 2100 W through the substrate, .5 ppm coating absorption and 2 ppm/cm substrate absorption.

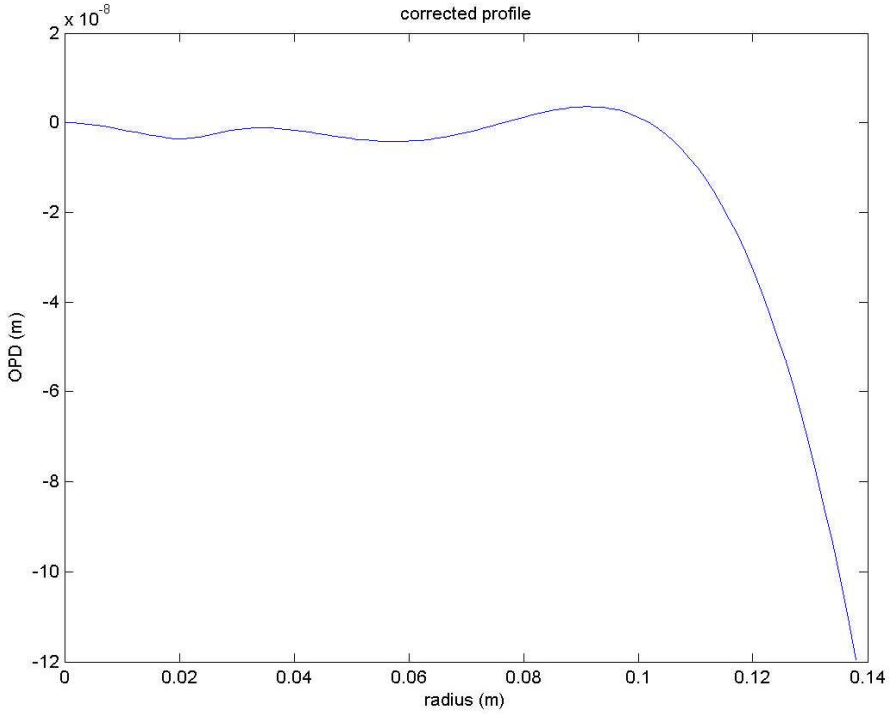

Figure 11: ITM phase profile after compensation by the heating pattern in Figure 11.

4.1.3 CO_2 Laser Projector

The CO_2 laser projector, being outside the vacuum, is easily adjusted to optimize its heating pattern. Our baseline design is for a fixed-mask staring projector. We also present a scanned projector concept that may be designed should the heating pattern need to be adjusted continuously.

4.1.3.1 Fixed-mask Staring Projector

This design is closely patterned on the CO_2 laser projector for initial LIGO, with the main exceptions being the projection of the beam onto the compensator plate, the use of a 25W laser, and the intensity modulation simultaneously from an AOM (for rapid intensity stabilization) and from rotating polarizers (for large dynamic range). The more powerful laser is chosen to give adequate headroom while not running the power modulating AOM at excessive deflection efficiency (where beam wander can be observed). Figure 12 shows the proposed layout. The mask design could be that for full compensation, as in initial LIGO, but might also be tailored to correct for manufacturing tolerance or deal with small inhomogeneities. In this latter case the precise mask illumination pattern cannot be predicted here. It will be devised using data from the Hartmann sensors *in situ* and/or from core optic metrology prior to optic installation. Optics with conical surfaces (‘axicons’) might also find use to efficiently convert the Gaussian beam of the laser to an annulus before further adjustment with the mask.

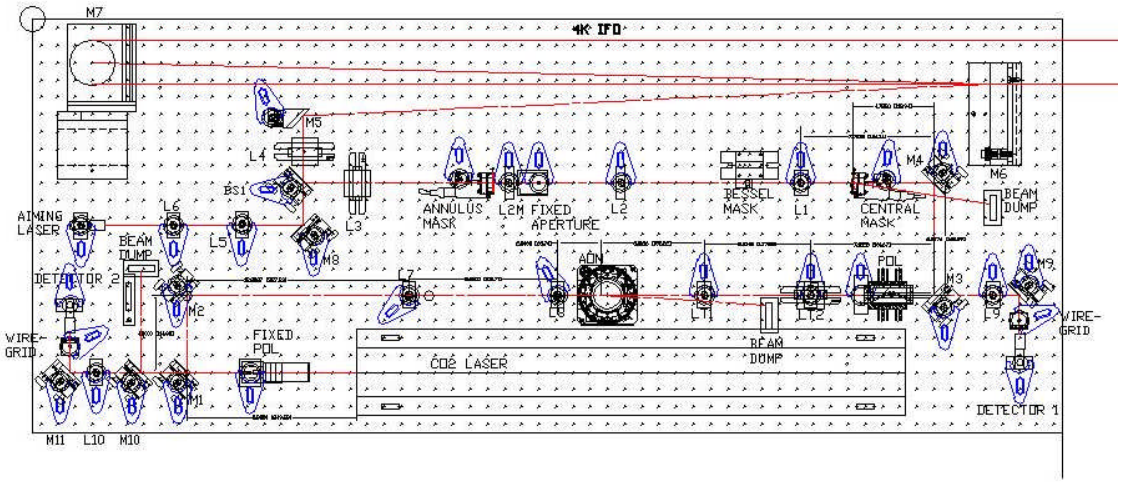

Figure 12: Fixed-mask staring CO2 projector

This design allows control only of the overall compensation intensity. This would make it easy to operate, though slow to modify- new masks would require at least a week to design and build. It is not clear whether or how often new masks would be required. The mask could either be the machined disks used in initial LIGO or ZnSe flats with reflective mask coatings on them for greater flexibility in compensation pattern.

The detector to be used is a Boston Electronics PVM-10.6 PD, with a noise floor of ~10^{-9}V/√Hz and a saturation level of ~10 mV, so power stabilization at the level of ~10^{-7}/√Hz looks feasible.

Since the CO_2 laser projector may need to make small adjustments to the compensation pattern for inhomogeneities in the optic absorption pattern, it is difficult to precisely predict how much power will be needed. The nominal 6 W of power absorbed by the optic from an optimized ring heater sets the scale for the CO_2 laser projector. The mask that converts a Gaussian laser beam to the optimal heating pattern is 24% efficient, so the CO_2 laser must provide at least 25 W. On the other hand, if the projector is to compensate for a 1 mm^2 spot that absorbs an excess 1ppm (that is, .14 mW excess heat if this spot is at the optic center), it will do this by radiating the same .14mW/mm^2 over the rest of the optic, which would require 9 W total. Therefore, a 25W laser is expected to be adequate.

4.1.3.2 Scanned Projector

Ryan Lawrence's original design for a CO_2 laser projector used an intensity-modulated beam scanned across the optic in a spiral raster pattern using galvanometer mirror deflectors. While this technique did provide thermal compensation of a point heat source (and by implication, of a more general heat source), his noise analysis did not correctly consider the presence of upconversion noise in the LIGO bandwidth, which would be severe. See Section 8.2 for analysis.

A scanned laser system is still possible. One technique would be to scan the laser across the optic face at much higher frequency, using acousto-optic modulators rather than galvanometers. This would have two advantages: the scanning frequency and all harmonics would be above the LIGO bandwidth, and the injected noise would be smaller, as it scales linearly with pixel dwell time, and thus inversely with scan frequency.

The limitation in this case arises if the injected phase noise has sufficient amplitude to drive the optical system outside its linear operating range. For example, if the injected optical path variations are at the 60 pm level, this corresponds to 350 microradians at 1.064 microns. The linear range of a cavity locking scheme is of order of $2\pi/\mathcal{F}$, where $\mathcal{F}$ is the cavity finesse. For Advanced LIGO, the finesse of the arms is about 730, for a linear range of order 8600 microradians.

The overall intensity of the CO_2 laser projector in the LIGO bandwidth must still be stable to a RIN of order $10^{-7}/\sqrt{Hz}$, which may be a serious challenge in a system modulated at high frequency.

4.1.3.3 In-vacuum Optics

A conceptual layout of the CO_2 laser projector optical beams is shown in Figure 13 for an unfolded interferometer. The CO_2 laser beam originates at the TCS table, shown in yellow, enters the vacuum through a viewport in the ITM BSC chamber and is sent by a steering mirror to a steering mirror low in the BS BSC chamber, where it is reflected back to the CP to impinge at roughly 7° from normal incidence. The CO_2 laser beam may be slightly diverging when it enters vacuum (as it does in initial LIGO), but for the sake of keeping the in-vacuum optics small the final steering mirror may also have magnifying power.

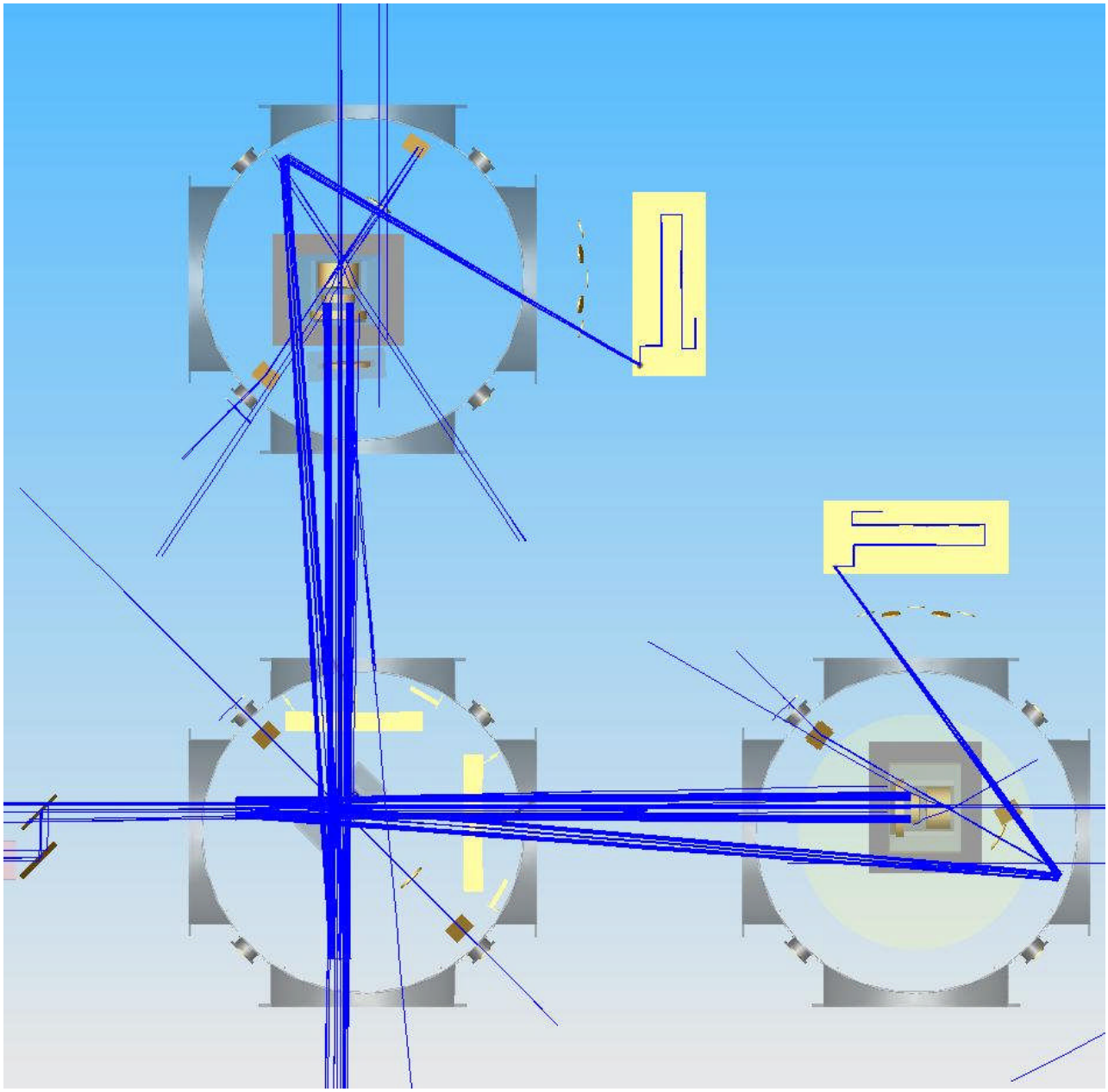

Figure 13: In-vacuum optics of the CO2 laser projectors.

4.1.4 Folded IFO TCS Actuator Design

In the folded interferometer, there is no conveniently long optical path from the CP to allow the beam to expand from small size to fill the CP, so the beam will have to expand faster, as well as impinge at a large incident angle from normal. Such a design appears feasible but must be developed in concert with the ITM/FM suspension assembly.

4.1.5 Simultaneous Compensation on the ITM and CP

The presence of thermal distortions simultaneously in the recycling cavities and arm cavities presents a problem for TCS design. As shown in Figure 8, when the test masses are compensated to maintain the arm cavity spot size at 6 cm, the resulting thermal phase profile of the ITM is not that for which the shielded ring heater on the CP was designed (Figure 9). However, if the test masses are not directly compensated, the arm cavity mode spot size shrinks to 5.4 cm, and once again the shielded ring heater on the CP is not optimal. Since the CO_2 laser projector will be sufficiently quiet for any heating pattern except possibly compensation of the ITM ring heater thermal lens, and a shielded ring heater cannot correct for the ITM ring heater thermal lens either, the design plan is to choose an drop the shielded ring heater, minimize the use of the ITM ring heater, and rely upon the CO_2 laser projector to apply all heating.[9]

4.1.6 Beamsplitter Compensation

There is no intention to directly compensate the beamsplitter. It contributes only ~10% of the thermal lens in the recycling cavities, and its effect can be largely compensated at the compensation plates. However, since the beamsplitter contributes different amounts of thermal lens to the power recycling cavity and to the signal recycling cavity, the whole effect of the beamsplitter thermal lens cannot be corrected for both recycling cavities at once at the compensation plates. This may not prove to be a significant problem. However, the option to retrofit thermal compensation onto the beamsplitter is maintained in the AdLIGO optical layout.

4.2 TCS Sensors

The sensors used by TCS are in two classes: ‘dedicated’ sensors that nominally sense a single optic’s phase profile using an injected probe beam, and phase cameras that sense the spatial profile of the main IFO beam and its RF sidebands.

4.2.1 Dedicated Sensors

[Modified to reflect adoption of Hartmann sensors over WLISMI sensors]

The dedicated sensors consist of a wavefront sensing device, and a probe beam whose wavefront contains the thermal aberration information to be sensed. In section 3.1.2.6 the TCS Design Requirements Document states that the wavefront sensor shall probe the central region of the ITM and CP to a radius not less than 112 mm.

4.2.1.1 Probe Beam Layout

In this section we present a conceptual layout of the in-vacuum optics for the dedicated sensor probe beams, and describe the tradeoffs that motivate the conceptual design.

4.2.1.1.1 ITM/CP Sensor

The most significant thermal aberrations are in the ITM/CP pairs, and their dedicated sensors are the most critical. If these sensors can probe collinearly with the main interferometer beam there

[9] Test Mass Thermal Compensation Strategies, LIGO document LIGO-T060215-01-D.

will be no parallax between the ITM and CP. The optimally compensated thermal phase profile will be flat, making no change to the inherent phase profile of the optics, and the phase measurement can be relative rather than absolute- any errors in the measurement of the cold optic are reproduced in the measurement of the hot optic and can be subtracted as an offset. This is strictly true only if the beamsplitter contributes no thermal aberration, which is not the case. However, the beamsplitter thermal lens is expected to be only ~5% of the ITM thermal lens, so the optimally compensated profile will have very modest lensing introduced by the BS. An off-axis sensor would have the same beamsplitter problem, in any case.

On-axis sensors require beam paths into the main IFO beam. We have two alternative designs which could satisfy requirements.

One is to use the wedged AR face of the beamsplitter. Figure 14 shows schematically how TCS ITM/CP sensor probe beams can be coupled into the main beam via these ghost beam rays. Note that to clarify the optical layout a horizontal wedge is shown. The real beamsplitter will have a vertical wedge. The implications for the design are not changed. Thanks to the beamsplitter wedge, this entry point effectively decouples the two ITMs as seen by the sensor probe beams. Take for example the sensor probe beam incident on the BS AR surface from the vicinity of the signal mirror (to the right). This beam descends to meet the BS, so that upon reflection from the wedged AR surface it is collinear with the main IFO beam directed toward ITMx (upward). By contrast, the probe beam passing through the beamsplitter continues descending as it approaches ITMy (at a lesser rate, due to the wedge) and misses ITMy completely. To first order, this probe beam does not see ITMy.

The probe beam for ITMy is more problematic, since the probe beam (incident on the BS from below, near the PRM, and incoupled by reflection off the BS AR face) must be coaxial with the main beam in the beamsplitter substrate before it transits the HR face on the way to ITMy. Part of this will be reflected from the BS HR face and probe ITMx.

This problem can be avoided if the sensor probe wavelength is fully transmitted by the BS HR face. By designing the BS HR coating and choosing the probe wavelength such that the BS HR face has T>99%, the light coupled to the wrong ITM is attenuated >10,000x upon return to the dedicated sensor relative to the desired beam.[10]

In addition, there are higher-order beams that circulate in the recycling cavities with the main beam more than once before coupling out at the BS AR face. Because these higher-order paths undergo many more reflections from partially reflecting optics, they will be attenuated, very much so if the BS AR surface can be made nearly perfectly reflecting for the probe beam. In addition, the probe beam will be angled very slightly to the ITM/CP axis. This angle will cause a deflection of the return beam from the incident beam, and since all higher-order probe beam paths are longer than the first-order path they will receive more deflection and can be separated and dumped. Models show that .05° tilt will be adequate for this purpose, and the parallax introduced thereby is only 260 microns.

One of the TCS dedicated sensor beams can share the POB telescope if it is installed on one of the correct ports of the beamsplitter.

[10] Assuming the light combines incoherently at the BS.

Given the condition that the BS HR face be highly transmitting for the TCS sensor probe beam, there are other injection schemes possible. For example, the TCS sensor probe beams can be injected through the rear face of one mirror in each mode-matching telescope. This would have the disadvantage of passing the TCS sensor beams through the recycling mirrors twice before they are detected, sacrificing power. It would have the advantage that the sensor beam telescopes could then be much smaller, saving cost, space, and weight. In a stable recycling cavity design that incorporates the mode matching telescopes inside the recycling cavities, the loss of power at the recycling mirrors is not a problem. However, the input optics will themselves be exposed to large variations in laser power as the interferometer is turned on, creating their own thermal lenses, which must be considered. No such problem exists for the output mode-matching telescope.

At present, there is no quantitative requirement on the HR and AR reflectivities of the core optics at the probe wavelengths.

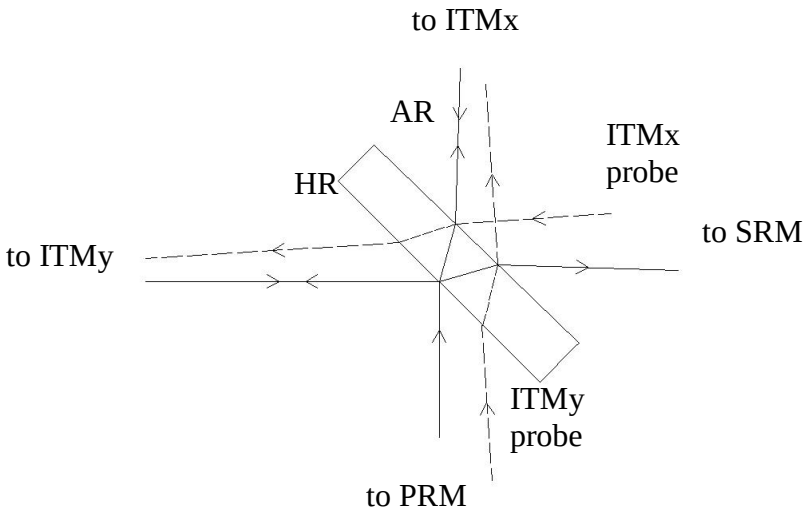

Figure 14: Configuration of dedicated sensor probe insertion points at beamsplitter. The solid lines show the paths of the main IFO beam. The dotted lines show the paths of the injected probe beams (except where they overlap with the main IFO beam.

Figure 15 shows an optical layout of the steering mirrors and beam expanding telescopes for the ITMx sensor. Stray light considerations require the actual telescopes to be reflectors rather than the refractors shown here- the reflective design would not differ essentially from the Pickoff Telescope design.

The ITM sensor probe beams will also sample the beamsplitter thermal aberrations in this geometry. The effect upon the wavefront sensor depends upon the sensor type and is discussed in Section 4.2.1.2.

Some power from the main IFO beam will also be present at this pickoff port. It will be necessary to strip this light from the probe beam with a hot or cold mirror and dump it consistently with the requirements for Stray Light Control. Likewise, the TCS probe beam will need to be stripped from the pickoff and ASP signals, again using dichroic mirrors.

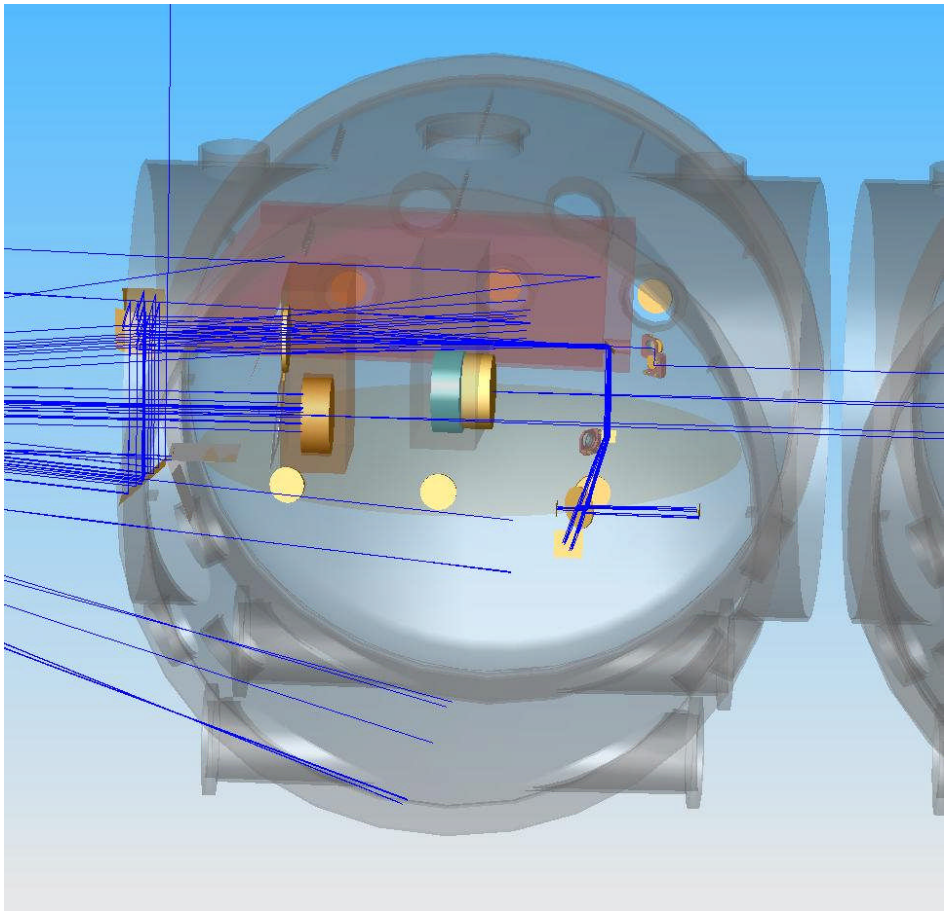

Figure 15: Steering mirror and telescope layout for the ITM CP sensors. The probe beam enters vacuum at the lower right, is raised by a periscope in the vacuum, is expanded by the telescope above the SRM as it travels to the left, and is steered down by a periscope to slightly below the optical table for injection to the BS AR face.

4.2.1.1.2 Beamsplitter sensor

TCS will also individually probe the beamsplitter. On-axis measurement of the beamsplitter phase profile is not possible, given the complex optic/beam geometry. The main function of the beamsplitter sensor is to provide a means to quickly identify gross departures from normal behavior.

Figure 16 shows phase profiles expected for sensor double-passing through the BS with a reflection from the HR face, one for 25 mW of bulk heating, and another for 25 mW of HR surface heating. The measurable difference between the two phase profiles allows us to distinguish the two heating patterns, which allows us to better estimate how the beamsplitter thermal aberrations contribute unequally to the two arms and two recycling cavities.

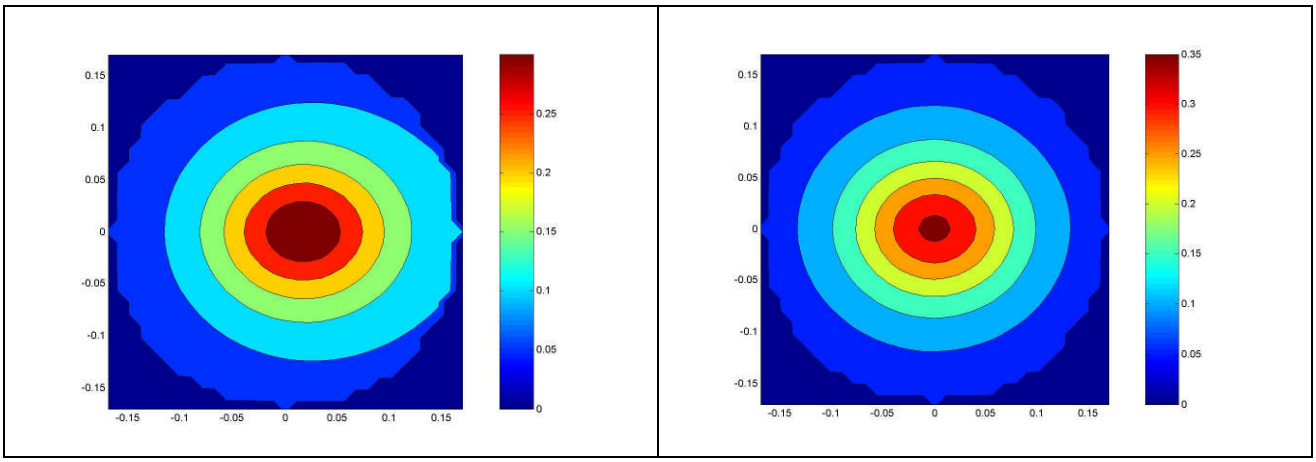

Figure 16: On-axis beamsplitter phase maps- the color scale indicates radians of phase. On the left, 25 mW bulk heating from homogeneous absorption. On the right, 25 mW uniform HR surface absorption.

The in-vacuum optical layout of the dedicated beamsplitter sensor is shown in Figure 17. The probe beam enters the bottom viewport at the lower left of the picture and is coupled by a periscope into the beam expanding telescope under the beamsplitter. Note that, since there are no IFO ghost beams in this direction, a refractive telescope may be used. A second periscope raises the expanded probe beam to the level of the beamsplitter face and directs it for retroreflection. The paths of the probe ghost beams are also shown in the figure not to interfere with the measurement.

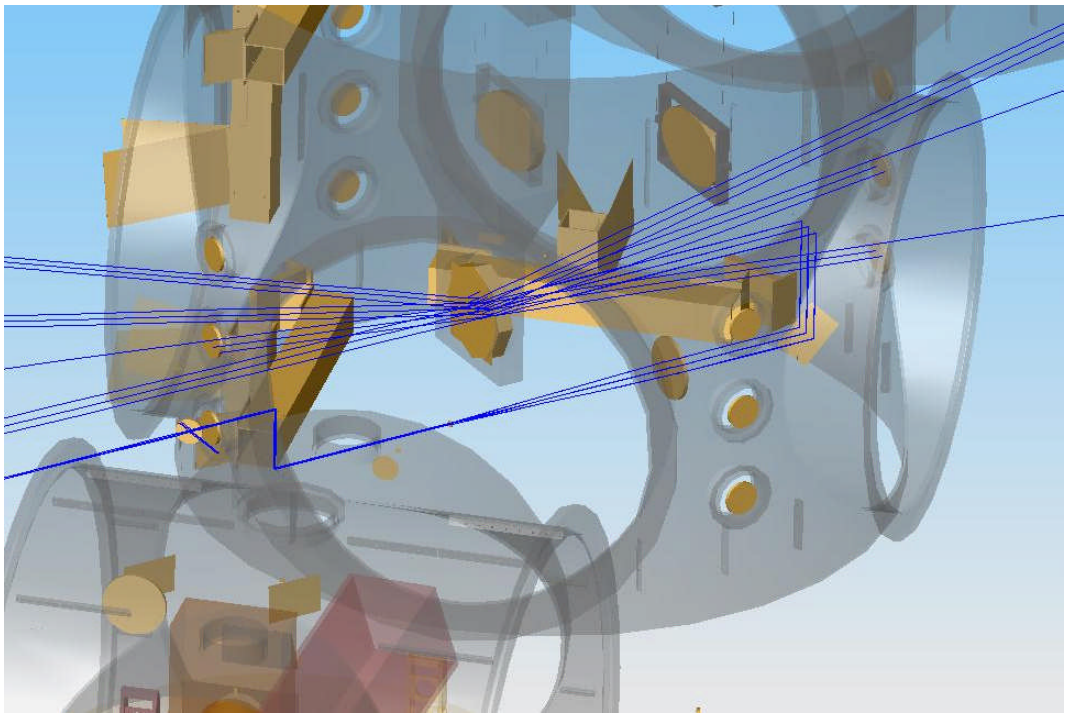

Figure 17: Dedicated beamsplitter sensor probe beam optical path. The ghost beams from unwanted reflections are also shown.

4.2.1.1.3 Test Mass HR surface sensors

It is not possible to probe the HR faces of the test masses on-axis, since that would require pickoffs inside the arm cavities. Since the TM HR surfaces are essentially planes, there is no parallax, and off-axis sensors give unambiguous results.

The optical layout of the off-axis reflective sensor beam is shown in Figure 18 for the two ITMs. After the expanded beam reflects from the TM HR face, it is retroreflected back into the telescope by an in-vacuum mirror, making this a double-pass measurement. For the ETMs, the transmission telescopes will be used to couple sensor beams on-axis through the AR face. Although the ETM sensor will predominantly measure thermal lens rather than thermoelastic deformation, this will still be adequate to measure total absorbed power, from which surface deformation can be inferred. This saves the cost of several telescopes. As for the beamsplitter, since there are no IFO ghost beams incident on these telescopes, refractive optics may be used.

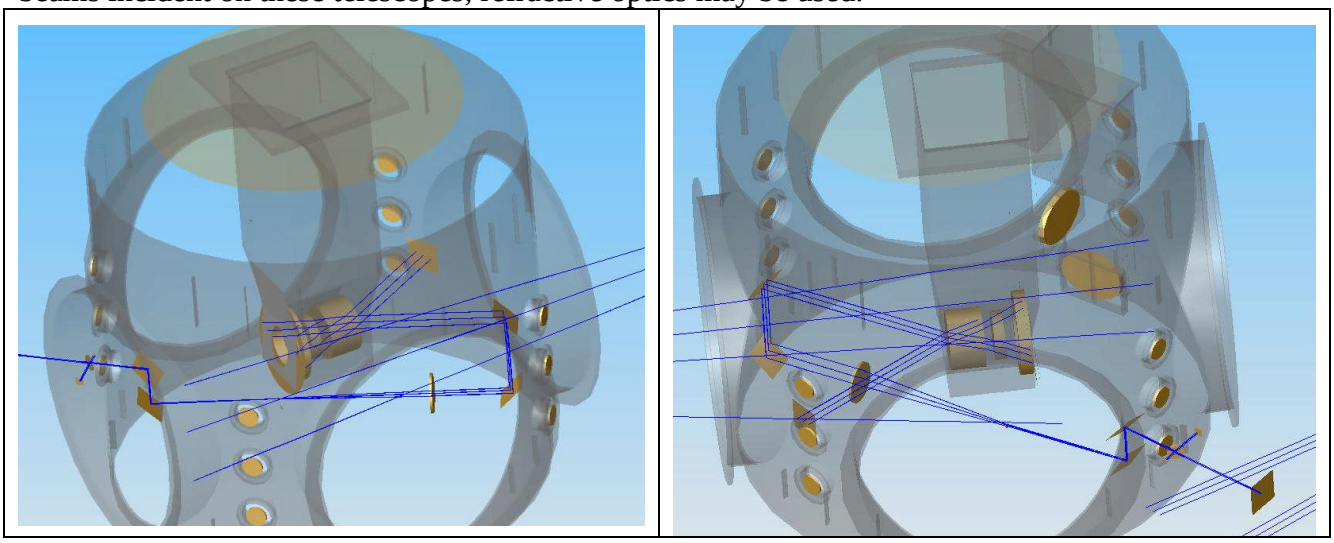

Figure 18: Layout of ITM HR surface sensors.

From Figure 3, we expect the magnitude of the surface deformation at full power to be of order 50 nm. Given the double-pass probe above, and assuming a S/N ratio of 10 to be desirable for this measurement, this indicates a wavefront sensor resolution of 10 nm. Assuming 635 nm probe wavelength, the wavefront sensor must have $\lambda/64$ precision. This would be easily met by a sensor sensitive enough for the ITM/CP.

It is not anticipated that the test mass HR surfaces will need to be continuously monitored as part of a TCS servo. Rather, the sensor will act as an aid to commissioning and a diagnostic should it be needed. Therefore, the TCS conceptual design envisions only one sensor per site, which can be relocated when necessary to the appropriate test mass. Should continual monitoring be needed, additional sensors can be built. Of course, in-vacuum optics will be built for all TMs.

4.2.1.2 Dedicated Sensor Conceptual Design

The main TCS sensor requirement, as described in Section 3.1.2.6 of the TCS Design Requirements Document, is that it sense the ITM/CP optical path to better than $\lambda/467$, where λ=1064 nm, on a grid with pixel spacing no greater than 1 cm, covering the central region of the optic to a radius no less than 112 mm.

The Advanced LIGO dedicated TCS sensor will be a Hartmann sensor.[11] Ryan Lawrence used a Shack-Hartmann sensor in his prototype tests of thermal compensators for Advanced LIGO- while it worked, he found it to be very fussy to align. The group led by Jesper Munch at the University of Adelaide, Australia, has been developing a Hartmann sensor for the Gingin experiment and as a potential wavefront sensor for Advanced LIGO. This latter device has been demonstrated to have adequate precision for Advanced LIGO and is described here.

A Hartmann sensor is simply a CCD camera with a multiple-aperture mask between it and an incident optical wavefront. The light spills through the apertures in the mask and falls upon small clusters of pixels on the CCD. As the wavefront of the incident beam varies, so does the propagation direction of the incident light through each aperture, and the light falls upon a slightly different cluster of pixels. The sensitivity is a function of such parameters as pixel size, individual pixel sensitivity, aperture size and spacing, and the distance from the mask to the CCD. A Shack-Hartmann sensor replaces the aperture mask with a lenslet array that focuses the beamlets onto the CCD. It is more efficient with incident light but more difficult to align.

The University of Adelaide's Hartmann sensor has been demonstrated to have a shot-to-shot reproducibility of $\lambda/580$ at 635 nm, which can be improved to $\lambda/16000$ with averaging, and with an overall accuracy of $\lambda/6800$. Since it is precision rather than accuracy that we are after in our sensors, the Adelaide Hartmann sensor meets the requirements for sensitivity quoted in Section 4.2.1.2.[12]

Advanced LIGO also requires the sensor to probe a region on the ITM/CP pair of radial extent not less than 112 mm radius, with a beamlet-to-beamlet spacing not greater than 5 mm. This is uniformly covered by 1576 pixels.

The Adelaide Hartmann sensor uses a 20x20 pixel segment on the CCD to measure each beamlet, so the number of beamlets is limited by the number of CCD pixels, and thus at least 630,000 pixels are needed to sample the full region. This is slightly less than the standard 768x1024 pixel array used by many CCD cameras, including that in the Adelaide prototype, and far less than the multiple Mpixels available in many modern CCD cameras. Therefore, the application of the Adelaide Hartmann sensor to Advanced LIGO TCS appears sound.

One complication is that there will be of order milliradian wedges built into some recycling cavity substrates to stifle parasitic etalon effects. These will produce ghost beamlets at the large optic of the beam expanding telescope that will be separated by only ~8 mm/milliradian from the main beamlets, potentially with many orders. If they have sufficient power, the ghost beamlets could confuse the measurement.

Another complication is the sampling of the beamsplitter thermal aberrations by the ITM sensor probe beams. The ITMx sensor reflects from the BS AR face from vacuum and therefore samples the thermoelastic deformation of that optic. The ITMy sensor reflects from the BS AR face from the substrate side and so samples the thermoelastic deformation and the thermorefractive aberrations in the beamsplitter. The absorbed power in the beamsplitter is less than 5% of the ITM

[11] RODA: Decision to adopt Hartmann sensors over WLISMI sensors for Advanced LIGO TCS, LIGO document LIGO-M070025-00-Y.

[12] Ultra-sensitive wavefront measurement using a Hartmann sensor, Aidan Brooks, Peter Veitch, and Jesper Munch, submitted to Applied Optics.

absorbed power, so the effect is small, but probably not ignorably small. Due to this incoupling of beamsplitter aberration the ITM/CP phase profiles will not be perfectly flat for ideal compensation. The departure from flatness can be determined from the dedicated beamsplitter phase sensor.

4.2.2 Phase Camera Design

The phase cameras in Advanced LIGO can be close analogs to the phase cameras in initial LIGO, or even direct copies of them. The chief difference between Advanced LIGO and initial LIGO as they relate to the phase cameras is that Advanced LIGO will use much larger RF modulation frequencies- as high as 180 MHz[13]. Since the photoreceiver has 1 GHz bandwidth, this makes no practical difference.

As designed, the phase camera has two somewhat undesirable features. One, the galvanometer mirror used to scan the pickoff beam across the photoreceiver generates vibrations that can couple into the optical table and disturb nearby equipment. Two, the galvanometer speed limits the scan rate to one per half second. Both of these problems can be removed if instead of a galvanometer a crossed pair of AOM deflectors is used to divert the beam. For the same 4000 pixel scans, a crossed AOM pair should require less than a millisecond. Another convenient feature that will be employed whichever scan technique is adopted is the mixing of the pickoff beam with a sample of the main laser beam offset by a AOM to a frequency that produces a distinct beat frequency with every component of the pickoff beam. This sample can be directed to the phase camera via and optical fiber and expanded to produce a nearly flat field, further simplifying the analysis of the phase camera images.

An alternative to the scanned image phase camera concept has been proposed by Rana Adhikari. He notes that 1064nm-sensitive CCD cameras with bandwidth in the MHz range are on the verge of commercial availability.

The phase cameras can be installed at any of a number of pickoff ports for the main beam, although POB, POY, and ASP are likely to contain the most useful information about thermal aberrations. We propose that the phase camera replace the bullseye sensor currently used in LIGO for TCS common mode control, since it measures the same quantity.

[13] "Optical Layout for Advanced LIGO," Dennis Coyne, LIGO-T010076-01-D, section 2.

5 Notes on Sensor and Actuator Beam Distortion

One practical design question relates to the beam expanding telescopes inside the vacuum used by the TCS dedicated sensors. Since the probe beam is large, distortion of the probe beam is likely unless the optics are very large and expensive, or multiple element telescopes are used.

It is our judgment that a significant amount of distortion can be tolerated in the TCS sensors. Take barrel distortion as an example. This will cause a Cartesian grid of pixels and the CCD plane to be imaged to a non-Cartesian pattern at the optic face with points away from the optic axis deflected further away from the optic axis. While the CCD camera sees a distorted picture of the optic's phase profile, this distortion is predictable, can be measured in the telescope before installation in vacuum, and can therefore be accounted for when analyzing the thermal phase profile of the optic in data processing. Therefore, it should make no difference to the operation of the TCS sensor.

A similar argument can be made for the CO_2 laser projector optics. The CO_2 laser projector beam must necessarily impinge upon the CP off-axis, introducing a foreshortening of the projected heat pattern that will easily be accounted for in the mask that produces the heater pattern. Distortion of the heater pattern can be dealt with in a very similar way.

Thus, while high quality, nondistorting optics are desirable for the TCS sensor and actuator beams, they are by no means essential. At present there are no quantitative requirements on the TCS sensor and actuator optical train distortion.

6 Notes on Thermal Depolarization

Generally, the thermal aberrations in fused silica optics are predominantly from thermorefractive effects, and secondarily from thermal expansion effects (the thermal expansion coefficient is only 6% of the thermorefractive coefficient). Fused silica also has a stress-optical coefficient, which can also contribute to thermal aberrations, but this effect is only 1% as large as the thermorefractive effect, and so introduces insignificant aberrations. However, the stress-optical effect does contribute a fundamentally different effect, in that the stress fields in the optic make it locally birefringent. Thus, light passing through the optic can be rotated into the orthogonal polarization, with the degree of rotation varying over the mode profile.

The amount of light lost to the orthogonal polarization in the ITM without compensation has been calculated by Efim Khazanov's group at the IAP to be 4.5 ppm. This is so much less than the pickoff reflectivity that it can safely be ignored. The amount of thermal depolarization in a compensated ITM/CP pair has not been calculated but is very likely to be of this order.

The depolarization could potentially be magnified if it coherently builds in the recycling cavity beam over multiple round trips. This effect has not yet been considered in detail.

7 Installation, Commissioning, and Control of TCS

In initial LIGO, the staring CO2 laser projector pattern is fixed by the mask, and the only control over the degree of thermal compensation is the CO2 laser power to the two ITMs. The common-mode TCS heating is chosen to optimize the RF sideband power in the recycling cavity, and is servoed using a bulls-eye photodetector which senses the pickoff beam size. The differential-mode TCS heating is chosen to minimize the unwanted AS_I signal at the dark port. The precise origin of the TCS-AS_I coupling is not well understood, and the gain of this servo changes significantly with IFO input power, even to the point of changing sign.

The ideal TCS servo would sense the spatial profile of the main IFO beam and dynamically reconfigure the spatial profile of the TCS actuator to maintain it at some nominal state. Unfortunately, there is currently no conceptual design for a thermal compensator with a dynamically tunable spatial profile that gives good compensation but does not inject a great deal of noise into the IFO. And, there is currently no known way to extract information from the IFO beam profile to tell TCS what spatial pattern of heat to apply to which mirror, with what power. This latter problem is what motivates the use of dedicated TCS sensors.

Nevertheless, without dynamic control of the heater spatial profile, and without any information about the thermal phase profile of the ITMs, TCS works quite well on initial LIGO, and did even when the heating of H1 was nearly half of what is expected in Advanced LIGO.

7.1 Installation and Commissioning

The installation and commissioning phase of TCS will go as follows:

1) *Characterize the core optics*.

Each core optic and compensation plate will have an absorption map of its coating and substrate, properly registered to the orientation the optic will have when suspended in the interferometer. This absorption map will be input to a finite element thermal model to predict the expected thermal phase profile for various IFO laser powers and at various times. This information will be used along with the expected shielded ring heater profile to design spatial profiles for the CO2 laser projector. There will also be reflection phase maps of the optics to aid in commissioning the dedicated TCS sensors.

2) *Design the initial CO2 laser projector profile.*

The information from the predicted thermal profiles will be used to design spatial profiles for the CO2 laser projector.

3) *Characterize the in-vacuum steering mirrors and telescopes.*

At this stage, the effects of distortion and other aberrations can be measured in the optics laboratory, for use later in qualifying the TCS dedicated sensors.

4) *Characterize the dedicated TCS sensors.*

At this point the TCS sensors can be tested against a reference flat either with or without the in-vacuum optics, as desired.

5) *Install the ring heaters and compensation plates with the test mass suspensions.*

At this stage, the centering of the CP and the ring heater will be assured.

6) *Install the in-vacuum steering mirrors, telescopes, and viewports.*

At this point, the location of the optical axis through the in-vacuum optics to the ITMs and BSs can be measured to aid in centering the dedicated TCS sensors.

7) *Install the dedicated TCS sensors.*

At this point the mapping of the optic face to the detector plane of the TCS dedicated sensors will be done.

Step 7 is the last stage of the TCS commissioning when access to equipment inside the vacuum chamber is required.

8) *Characterize and install the CO2 laser projectors.*

With the TCS dedicated sensors available, the centering of the projectors will no longer rely on the red laser diode crosshair projector, as it did in initial LIGO. The crosshair projector will be used only for rough alignment. A test-pattern mask (perhaps simply a small central crosshair) will be projected onto the CP and sensed by the TCS dedicated sensor for correct alignment.

9) *Install the servo electronics for the CO2 laser projectors, TCS dedicated sensors, and ring heaters, and the phase cameras.*

From this point forward, the TCS commissioning will require that the interferometer be under vacuum.

10) *Adjust the heaters to make sure the TCS sensors and actuators yield results consistent with predictions on individual optics.*

This stage is meant to verify end-to-end that a TCS actuator can produce a signal observable by the corresponding TCS dedicated sensor as expected.

From this point forward, the TCS commissioning will require some optical power circulating inside the interferometer.

11) *Lock the interferometer at low power and measure the self-heating with the TCS sensors; test the compensation with the ring heaters and CO_2 laser projectors.*

If the initial estimate of the optimal CO_2 laser projector heating pattern is incorrect, it is likely to be discovered at this point. Phase profiles can be measured with the TCS dedicated sensors and used to devise improved heater spatial profiles. If any optic is absorbing dramatically differently than expected based on the data in step 1, it will also be discovered at this point.

12) *Revise the CO_2 laser projector heating profiles and repeat step 11).*

This step is likely to be repeated several times as the IFO power is increased and the rest of the interferometer commissioning progresses, depending on how good the TCS performance needs to be at the moment.

We are likely to implement a servomechanism for controlling the TCS power levels to the various optics. Given the initial LIGO experience, and in the absence of a detailed model of interferometer performance, it is difficult to specify what that strategy will be, but does not represent a daunting task. The first approach will likely involve using the dedicated sensors to measure the compensated optic phase profiles and generate an error signal based upon their overall difference

from the cold phase profile, parameterized in some way. This approach has been demonstrated using a scanning CO2 laser projector compensator on an individual optic by Ryan Lawrence with good results.

7.2 Differential Control

In initial LIGO, the differential-mode TCS level is chosen to keep the AS_I signal at the dark port low. With its homodyne readout scheme, Advanced LIGO will not have an AS_I signal, and the differential TCS will be set by another consideration, the dark port power. It is very difficult to precisely specify the performance required by TCS in this regard, although we expect that the requirement will be easily met.

Ryan Lawrence used Melody to analyze the total power at the dark port when differential thermal effects between the two arms were present. Most of the stray light was in higher-order modes, which would then increase the shot noise at the output photodetector. Lawrence's model was correct as posed, but there are significant differences between his model and Advanced LIGO: he did not consider signal recycling, an output mode cleaner, or the homodyne readout scheme. All three of these differences change the sensitivity of Advanced LIGO to differential thermal effects, generally making it less sensitive. Ryan Lawrence also did not consider the use of stable recycling cavities. While this may yet be an option for Advanced LIGO, we also do not consider them here.

The output mode cleaner is the most significant change. The output mode cleaner is planned to have finesse of order 100-1000, and a cavity length of order 30 cm. We adopt a finesse of 300 for this discussion.

For an exactly antiresonant mode, the power transmittance of the (lossless) output mode cleaner is $\sim 1 \times 10^{-5}$. In general, the transmissivity will be higher, but for all modes not within 5% of a free spectral range of resonance the suppression will be at least 2.8×10^{-3}. Adopting this latter value as typical, and assuming no significant higher transverse mode falls within 5% of resonance, then the requirement that no more than 1 mW dark port light come from higher order modes[14] means that no more than 357 mW can issue from the signal recycling mirror.

The addition of the signal recycling mirror is another complication. A full model of the dual-recycled interferometer, including thermal effects, is needed to analyze this in detail. However, rough estimates can be made here. The signal recycling mirror transmittance is 0.05; therefore, for no more than 357 mW junk light out of the signal cavity no more than 7.14 W of junk light can be incident on the signal recycling mirror.

The presence of the signal mirror will affect the power buildup of these transverse carrier modes- this effect has not yet been adequately modeled. However, Lawrence did model a thermally compensated fused silica Advanced LIGO without the signal mirror, and showed that the junk light did not exceed 1 W even with 50% differential absorption between the arms (see the second chart of Figure 19). More quantitatively, with 2100 W combining at the beamsplitter, the mode overlap must be better than 99.7% for the light due to contrast defect to be less than 7.14 W. Therefore, the ring heater design in 4.1.2 should satisfy this requirement as well[15].

[14] Section 3.1.2.4, TCS Design Requirements Document

[15] Ibid.

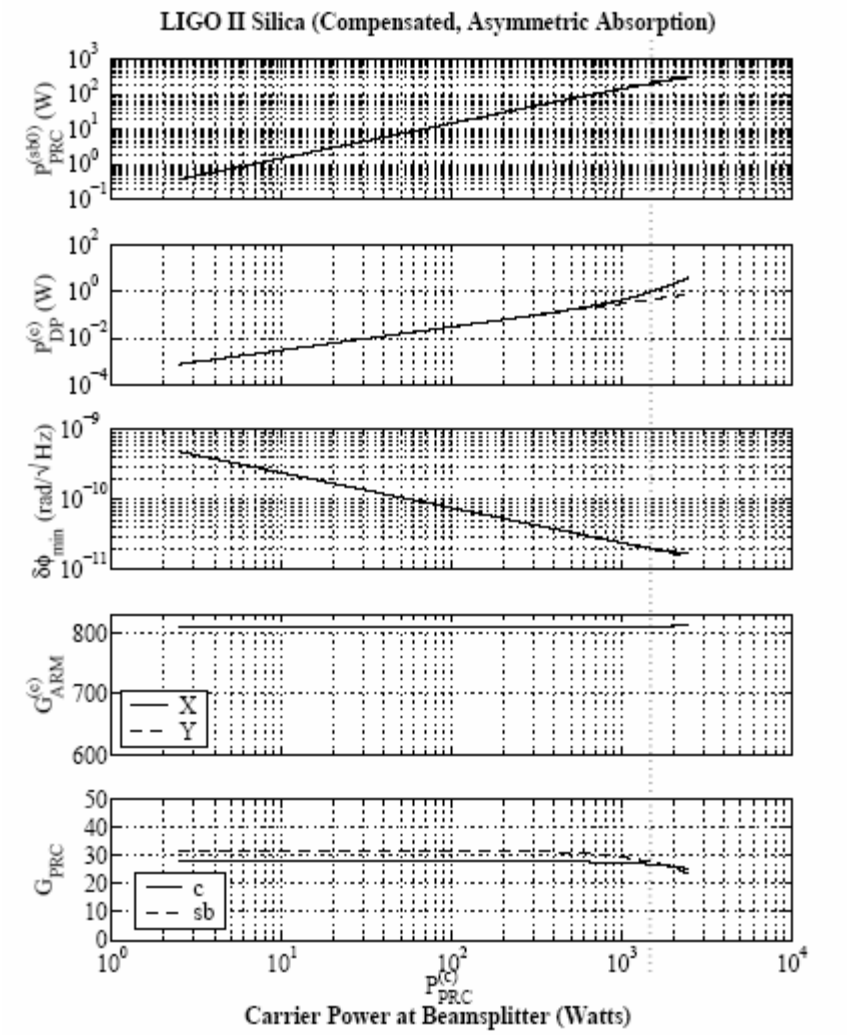

Figure 19: IFO performance with thermal compensation and no SRM. From Lawrence's thesis.

8 Appendices

8.1 Coupling of Test Mass Flexure Noise to Displacement Noise

A test mass ring heater changes the radius of curvature of a test mass's HR surface by flexing the mirror. Since the position of the center of the HR surface relative to the test mass center of gravity varies with the flexure, any noise in the ring heater power that can vary the flexure will create displacement noise. The details of this analysis are found in LIGO document T060224-00-D.

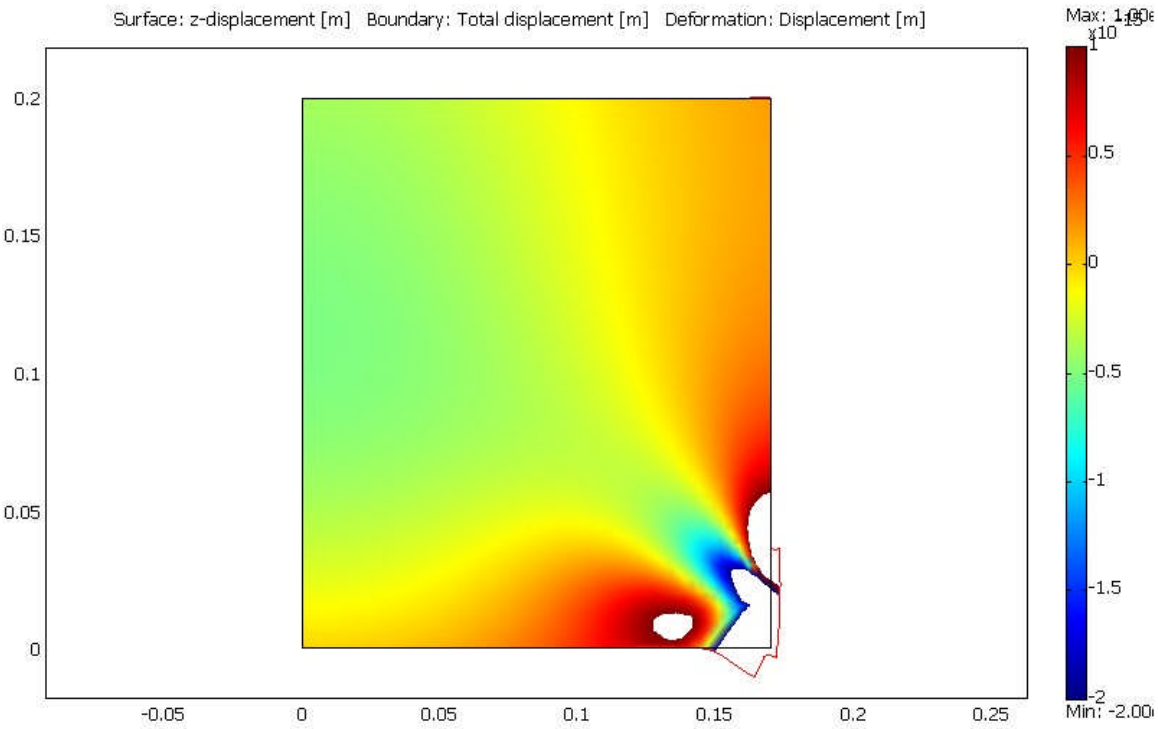

Figure 20: Thermoelastic deformation from 1 second of 100 W of barrel heating.

Figure 20 shows a cross section of the thermoelastic deformation of the test mass with 1 W, 100 Hz barrel heating (modeled using COMSOL). This model was used to estimate the flexure noise coupling by comparing the displacement of the center of the HR face ($4x10^{-16}$ m) to the displacement of the mirror center of mass, which is equal to the mean displacement over the whole mass ($2x10^{-16}$ m).

We require the TCS injected displacement noise to be less than $5x10^{-22}$ m/√Hz at 100 Hz, so this 1 W fluctuation must be scaled down to $2.4x10^{-6}$ W/√Hz. In order to fully compensate the arm cavity at high IFO power, it will be necessary to provide 22W of heat to the ETM, in which case we require $1.1x10^{-7}$/√Hz RIN. This should be simple to provide with a ring heater, whose thermal inertia will passively smooth power fluctuations on its input supply.

The full analysis of the flexure, elasto-optic, thermoelastic, and thermorefractive noise couplings in both the CP and the TM can be found in LIGO document T060224-00-D.

8.2 Scanned CO2 Laser Projector Noise

The scanned CO2 laser projector prototyped by Lawrence has not been adopted as the baseline design, because the analysis of the noise coupling in Section 5.2 of his thesis is incorrect. Because each 'pixel' on the test mass is visited briefly once every 6 seconds to receive a pulse of heat to maintain the pattern, the injected fluctuations are large, ~60 nm in a typical pattern. Lawrence's analysis assumes that since the highest frequency in the scan pattern is 6 Hz, the injections are safely below the Advanced LIGO bandwidth. This is true only if the injections are sinusoidal, or at least varying only at frequencies at and below the 6 Hz pixel rate. This is likely in practice to be a very finicky condition to achieve, and Lawrence's prototype does not even try, injecting constant power on each pixel when it is illuminated and no power when it is not, the heat injection thus being a sawtooth at each pixel.

Figure 21 shows a sample injected noise spectrum around 300 Hz for a scanned laser system with ~60 nm injected thermal actuation pulses, with the actuation pulse size randomly varied by a factor of two to mimic a typical actuation pattern. The figure shows that the injected noise in this case is broadband, and very large compared to the compensation plate noise requirement of ~10^{-19}m/√Hz as outlined in Section 3.1.3.1 of the TCS Design Requirements Document.

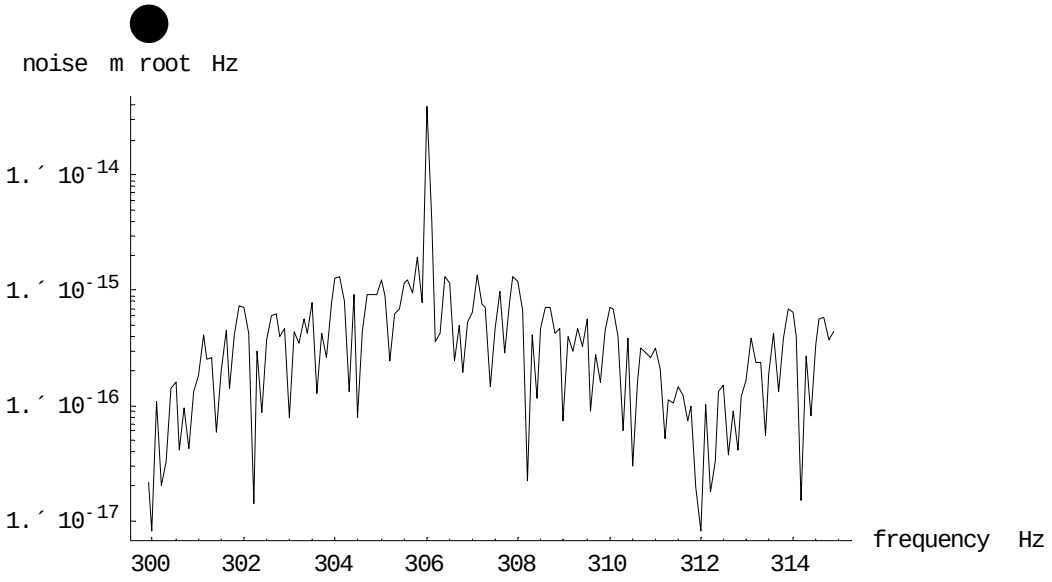

Figure 21: Sample injected noise spectrum from scanned carbon dioxide laser projector.

Injecting a sawtooth heating pattern is not a prerequisite of the scanned CO2 laser projector design. One could imagine tailoring the heating pattern to more smoothly ramp up and down as the heat scans from spot to spot. Nevertheless, this analysis shows that such an approach would require delicate tailoring to reduce the noise to acceptable levels.